ADVANCED FUNCTIONAL MATERIALS
www.afm-journal.de

Radiation Hardness and Defects Activity in PEA_2PbBr_4 Single Crystals

Andrea Ciavatti, Vito Foderà, Giovanni Armaroli, Lorenzo Maserati, Elisabetta Colantoni, Beatrice Fraboni, and Daniela Cavalcoli*

Metal halide perovskites (MHPs) are low-temperature processable hybrid semiconductor materials with exceptional performances that are revolutionizing the field of optoelectronic devices. Despite their great potential, commercial deployment is hindered by MHPs lack of stability and durability, mainly attributed to ion migration and chemical interactions with the electrodes. To address these issues, 2D layered MHPs are investigated as possible device interlayers or active material substitutes. Here, the 2D perovskite $(PEA)_2PbBr_4$ is considered that is recently discussed as promising candidate for X-ray direct detection. While the increased resilience of $(PEA)_2PbBr_4$ radiation detectors has already been reported, the physical mechanisms responsible for such improvement compared to 3D perovskites are not still fully understood. To unravel the charge transport process in $(PEA)_2PbBr_4$ crystals thought to underly the device better performance, an investigation technique is adapted previously used on highly resistive inorganic semiconductors, called photo induced current transient spectroscopy (PICTS). It is demonstrated that PICTS can reliably detect three trap states (T1, T2, and T3), and that their evolution upon X-ray exposure can explain $(PEA)_2PbBr_4$ superior radiation tolerance and reduced aging effects. Overall, the results provide essential insights into the electrical characteristics of 2D perovskites and their potential application as reliable direct X-ray detectors.

1. Introduction

The outstanding rise of metal halide perovskites (MHPs), driven by their photosensitive properties, impacts a broad class of optoelectronic semiconducting devices like photovoltaic solar cells, lasers, LEDs, and visible and X-ray photodetectors. MHPs offer great performance in terms of power conversion efficiency in solar cells and of sensitivity in photodetectors. However, stability and durability issues arise from ions moving in the perovskite layer under an external electric field (so called "ion migration") and to their easily triggered chemical reactions with metal electrodes and by the environment. To mitigate these aspects, 2D layered MHPs are being investigated as alternative or additive materials. 2D MHPs have been studied to stabilize solar cells in 2D single layer,[1] as 2D/3D bilayer,[2,3] or as passivating layer in 2D/3D mixtures.[4,5] Among them, the Ruddlesden-Popper halide perovskites with phenylethylammonium ($PEA^+ = C_6H_5C_2H_4NH_3^+$) as ionic cation were proven to be stable in high-vacuum environment and under X-rays,[6,7] and to be an excellent active material for UV photodetectors.[8] Thanks to these peculiar properties highly sensitive and ultra-stable direct X-ray detectors based on PEA_2PbBr_4 perovskite thin films have been recently realized and proven to effectively operate after 80 days in air and after a radiation stress test (exposure to ≈4 Gy of total X-ray irradiation).[9]

Furthermore, 2D perovskites proved their potential as stable X-ray direct detector in several formulation and device geometry. Quasi-2D perovskites with formulation $BA_2MA_2Pb_3I_{10}$ and $BA_2MA_4Pb_5I_{16}$ ($BA^+ = C_4H_{12}N^+$, butylammonium) are stable for tens of hours under bias and ionizing radiation both in thick[10] or thin[11] films. Another quasi-2D $PEA_2MA_8Pb_9I_{28}$ polycrystalline thick film showed very high sensitivity (10 860 μC Gy^{-1} cm^{-2}) and low detection limit.[12] As ordered system, single crystals of $(F\text{-}PEA)_2PbI_4$ have very high resistivity (>10^{12} Ω cm), high stability, and low noise thanks to suppressed ion migration due to supramolecular electrostatic interaction between electron-deficient F atoms with neighbor benzene rings.[13] The vast majority of studies on 2D perovskites are focused on the device performance and on the effect to the device signal stability (e.g., sensitivity, dark current, etc.) on aging, environmental stability and radiation hardness at low fluxes (few Grays). The few fundamental physical property investigations target the

A. Ciavatti, V. Foderà, G. Armaroli, L. Maserati, E. Colantoni, B. Fraboni, D. Cavalcoli
Department of Physics and Astronomy – Alma Mater Studiorum University of Bologna
Viale Berti-Pichat 6/2, Bologna 40127, Italy
E-mail: andrea.ciavatti2@unibo.it

The ORCID identification number(s) for the author(s) of this article can be found under https://doi.org/10.1002/adfm.202405291

DOI: 10.1002/adfm.202405291

materials' optical characteristics (absorption and photoluminescence) aiming at photovoltaic applications.[14]

So far, limited knowledge is available on the role and behavior of electrically active defects, and on their evolution with aging and under ionizing radiation. Shallow and deep in-gap electronic levels are of fundamental importance for the understanding and control of the semiconducting transport properties of materials. In-gap states investigation on inorganic semiconductors in the last 50 years played a major role for their technological development.[15] Deep Levels Transient Spectroscopy (DLTS) and Photo-Induced Current Spectroscopy (PICTS) are powerful techniques for the study of these electrically active defects in semiconductors.[16] In recent years DLTS and PICTS have been employed on lead-halide perovskites,[17,18] even if the interpretation of the results is still under debate,[19] and the identification of defects is challenging.[20] Several issues affecting DLTS/PICTS analyses of 3D perovskites arise from ion migration and its interaction with hole and electron transport. This leads to a difficult interpretation of the spectra that hinders a reliable identification and differentiation of electron traps and migrating ions. Thus, thanks to their superior stability and reduced ion migration, 2D perovskites represent an ideal laboratory to investigate electrically active defects, avoiding most of the concerns of DLTS/PICTS applied to 3D perovskites.[21] Moreover, single crystals, as ordered systems, are more prone to the identification of specific defect states, compared to polycrystalline or 2D/3D mixed systems. Finally, metal-Br perovskites are expected to have a smaller intrinsic charge carrier density (larger bandgap) compared to metal-I ones, and to be less prone to oxidation by environmental O_2, thus further improving time and radiation stability.

Here we investigate the role and evolution of electrically active defects in the prototype 2D perovskite PEA_2PbBr_4. To achieve this, we do not employ DLTS due its limitations on high resistivity semiconductors,[22] and instead we demonstrate the applicability of PICTS to 2D perovskites. Millimeter-size PEA_2PbBr_4 single crystals were synthesized, and their quality and stability demonstrated through UV and X-ray photo-response performance as-grown and after 1 month. Performing PICTS we retrieved stable and reproducible spectra. Three deep levels were clearly identified, and their evolution under 200 Gy of X-ray and over 1 year investigated and discussed.

2. Results and Discussion

2.1. Optoelectronic Properties of PEA_2PbBr_4

The growth of PEA_2PbBr_4 single crystals follows the slow solvent evaporation technique. Starting from the precursors PEABr and $PbBr_2$ the following reaction proceeds:

$$2\ PEABr + PbBr_2 \rightarrow PEA_2PbBr_4 \quad (1)$$

The precursors, mixed in stochiometric fractions, are dissolved in DMF (N,N-Dimethylformamide) solvent to form a 1:3 molar solution (slightly above the supersaturation value of the solute in the solvent). The solution is passed through 0.22 µm filters and put to rest in a beaker covered with Parafilm where small holes of about one millimeter of diameter were punched. Over days, as the solvent evaporation continues, the solute molarity passes the saturation threshold causing a single crystal to nucleate. After about three weeks, the PEA_2PbBr_4 crystal is grown to an approximately octagonal shape with sides ranging from a few millimeters to about one centimeter. Interdigitated metal electrodes are deposited through shadow mask by thermal evaporation of gold or chromium, with channel length L = 30 µm and total width of W = 18.23 mm (**Figure 1a**). In this architecture, the crystal behaves as photoconductor with co-planar electrodes.

The surface of the single crystals has been optically investigated through optical microscope under polarized light and through White Light Interferometer (WLI). The crystals show relative flat and uniform surfaces, as few holes area present under direct polarized light microscope (Figure SI 1a, Supporting Information); further, the picture with cross-polarized light is dark and uniform, indicating an absence of crystalline discontinuities (Figure SI 1b, Supporting Information). Further, White Light Interferometer (WLI) microscopy images highlight the size of the feature visible at the surface (Figure 1b; Figure SI 2, Supporting Information). They show: i) few holes, which height is below 1 micron; ii) occasional plane steps ≈2 µm height; iii) large region of flat crystal surface with roughness < 100 nm. Figure 1c shows the photoluminescence (PL) spectra collected changing the angle between the excitation source (nitrogen laser at 337 nm) and the samples. Angular-dependent measurements allow for deeper penetration of light into the crystal bulk when the source is at 90°, whereas at 45°, the excitation predominantly affects the surface region of the crystal. The PL spectra reveal two emission peaks at 415 and 435 nm. The emission peak at 415 nm is higher when the excitation angle is 45°, indicating that this peak is predominantly associated with surface emission. In contrast, the peak at 435 nm is more intense at 90°, suggesting it is primarily linked to the bulk response of the crystal.[23,24]

When an external voltage is applied to the electrodes, an electric field is present along the high-conductivity in-plane direction (i.e., the direction of inorganic $PbBr_6$ layers). Current-Voltage characteristics in dark and under the excitation of a 375 nm LED source are reported in Figure 1d. The metal electrodes form an ohmic contact with the crystal, with a very high resistance of $\approx 10^{12}$ Ω,[25] granting an extremely low dark current of few pA at 10 V. Despite the large exciton binding energy, the photocurrent response under UV illumination (LED at 375 nm) is very efficient, showing an on/off current ratio up to 10^4 at 0.8 mW cm^{-2} and a signal-to-noise ratio (SNR) equal to 440 already at 30 µW cm^{-2}. The Responsivity reaches 12 mA W^{-1}, in accordance with pure PEA_2PbBr_4 single crystals[8] and 20 times higher than the responsivity of polycrystalline PEA_2PbBr_4 films grown by spin coating (Figure SI 3, Supporting Information).[9] These values confirm the good quality of the crystals used in this study. In the photocurrent spectrum of Figure 1e two high signal regions are identified: the large exitonic peak at 3.02 eV and the continuous band. Appling the Elliott Formula[26,27] in the continuous region in the vicinity of the threshold, an energy gap E_g = 3.08 eV is determined with an excitonic peak ≈0.06 eV below the bandgap. The temperature-dependent electrical conductivity in the 200 – 340 K range follows the Nernst–Einstein equation, with one single activation energy (Figure SI 4a,b, Supporting Information) equal to 0.11 eV, meaning that only one crystalline

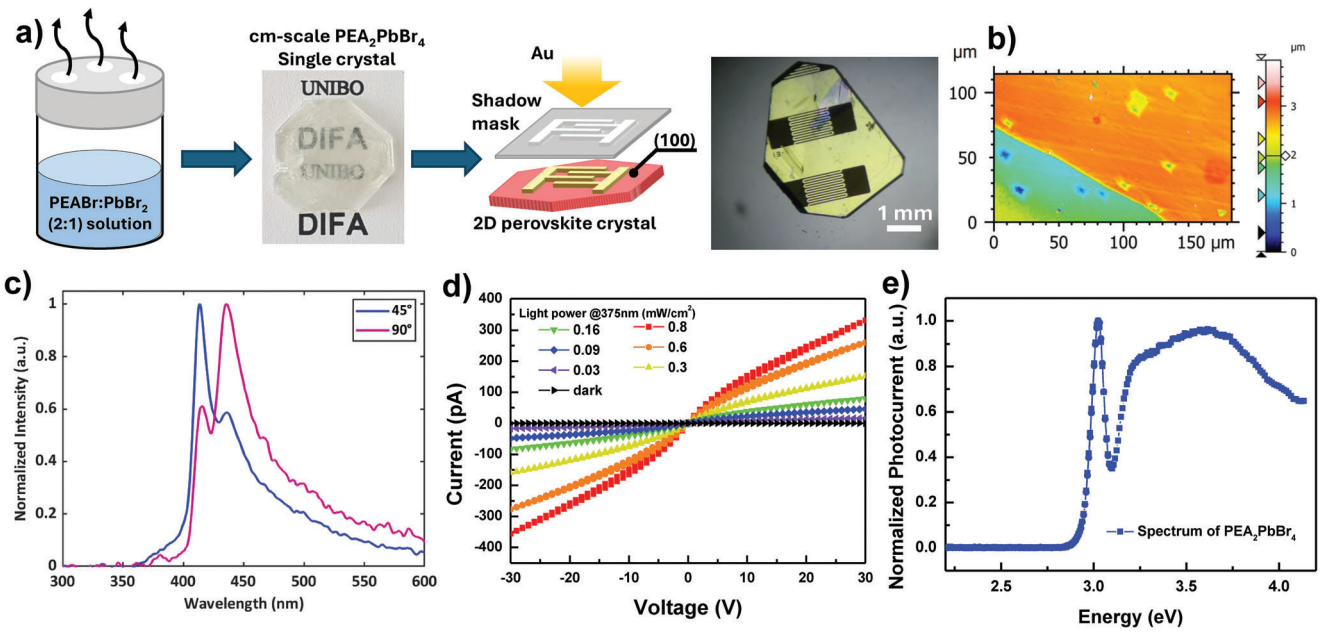

Figure 1. Device fabrication and optoelectronics properties. a) Sketch of device fabrication from crystal growth to electrode's evaporation and optical image of the device before wiring. b) White Light Interferometer colormap image of the crystal surface. c) Photoluminescent spectra with angular-dependence for 45° (blue line) and 90° (purple line). d) Current–Voltage characteristics of PEA_2PbBr_4 single crystals in dark and under 375 nm LED light. e) Normalized UV–vis photocurrent spectrum PEA_2PbBr_4 single crystals where large exciton peak and band edge are visible.

phase is present in the considered temperature range. On the contrary, 3D perovskites like $MAPbBr_3$ typically undergo crystal phase transitions and present two (or more) temperature ranges with different activation energies (Figure SI 4c, Supporting Information). In particular, high activation energies are extracted at high temperatures, associated to ionic transport.[28,29] Activation of ionic transport have been observed in PEA_2PbBr_4 only at temperature above 340 K,[21] much higher that 3D perovskite counterparts, indicating that close to room temperature (or below) the ionic transport is strongly reduced.

The response of the devices under X-ray has been tested at different voltages (5 – 50 V) and at different dose rates (2.5 – 25 μGy s^{-1}) under a W-target X-ray tube in the 40 – 150 kVp range, see **Figure** 2a,b. The crystals showed linear response to increasing dose rates for all applied biases, reaching a maximum of sensitivity of 64.8 ± 0.7 μC Gy^{-1} cm^{-2} at 50 V. Figure 2d reports the X-ray photocurrent response spanning over three orders of magnitude of dose rate, from 2.5 to 1330 μGy s^{-1}. Although the signal is continuous, PEA_2PbBr_4 crystals have small sublinear behavior equal to a slop of 0.75 ± 0.02 in Figure 2d for all the bias voltages. This effect it is well established in perovskite detector and several examples are present in literature.[9,30] Extending the range to lower dose rates, a minimum detectable dose of 200 nGy s^{-1} has been calculated (Figure SI 2, Supporting Information). To evaluate the mobility-lifetime product ($\mu\tau$) we acquire the signal output from the detector under the irradiation of an alpha emitting source of ^{226}Ra. The α-particles have a low-penetration depth in solid state materials, and they stop within few tens of microns from the impinging surface of the perovskite crystal. Due to the interdigitate geometry of the electrodes and to the layered structure of the 2D perovskite crystals, the charges are collected only close to the top surface where the metal electrodes were deposited. The use of α-particles allows to achieve full charge collection and to reach the saturation of photocurrent with the applied bias. Further, we consider uniform carrier generation linearly distributed throughout the channel length. Under these assumptions, the commonly used Hecht formula[31,32] could not be applied. We employ a specifically modified expression that considers uniform carrier generation[33,34] (see Technical Note 3). Figure 2c reports the experimental data and the corresponding photocurrent versus voltage fit, resulting in a $\mu\tau$ value of (1.96 ± 0.13) x 10^{-6} cm^2V^{-1}. Indeed, the general equation for uniform carrier's generation foresees the contribution of both positive and negative charges. However, in our architecture we cannot distinguish between them. Therefore, we should consider the $\mu\tau$ value evaluated from this coplanar structure as the sum of holes and electrons parameters.[35]

2D perovskites are generally considered stable materials in operating environment and under physical stress effects like external bias or impinging radiation. The $(PEA)_2PbBr_4$ single crystals presented in this work exhibited very good stability to radiation (Figure 2e) and aging (Figure 2f). Figure 2e reports the electrical resistance in dark conditions and the X-ray sensitivity before and after exposure to 200 Gy of X-ray irradiation at 150 kVp: the values are perfectly overlapped within experimental errors. Figure 2f displays X-ray photocurrent and sensitivity for as-fabricated crystals (t = 0) and for the same crystals after 30 days of storage in ambient conditions. Further optoelectronic properties, like sample resistivity in dark, photocurrent output at 10 V for 385 nm LED (ΔI), Responsivity (R) and Specific Detectivity (D*), have been monitored for as-grown crystals and after two years of shelf storage (Table SI 1, Supporting Information). The sample display remarkable stability in all of the above parameters.

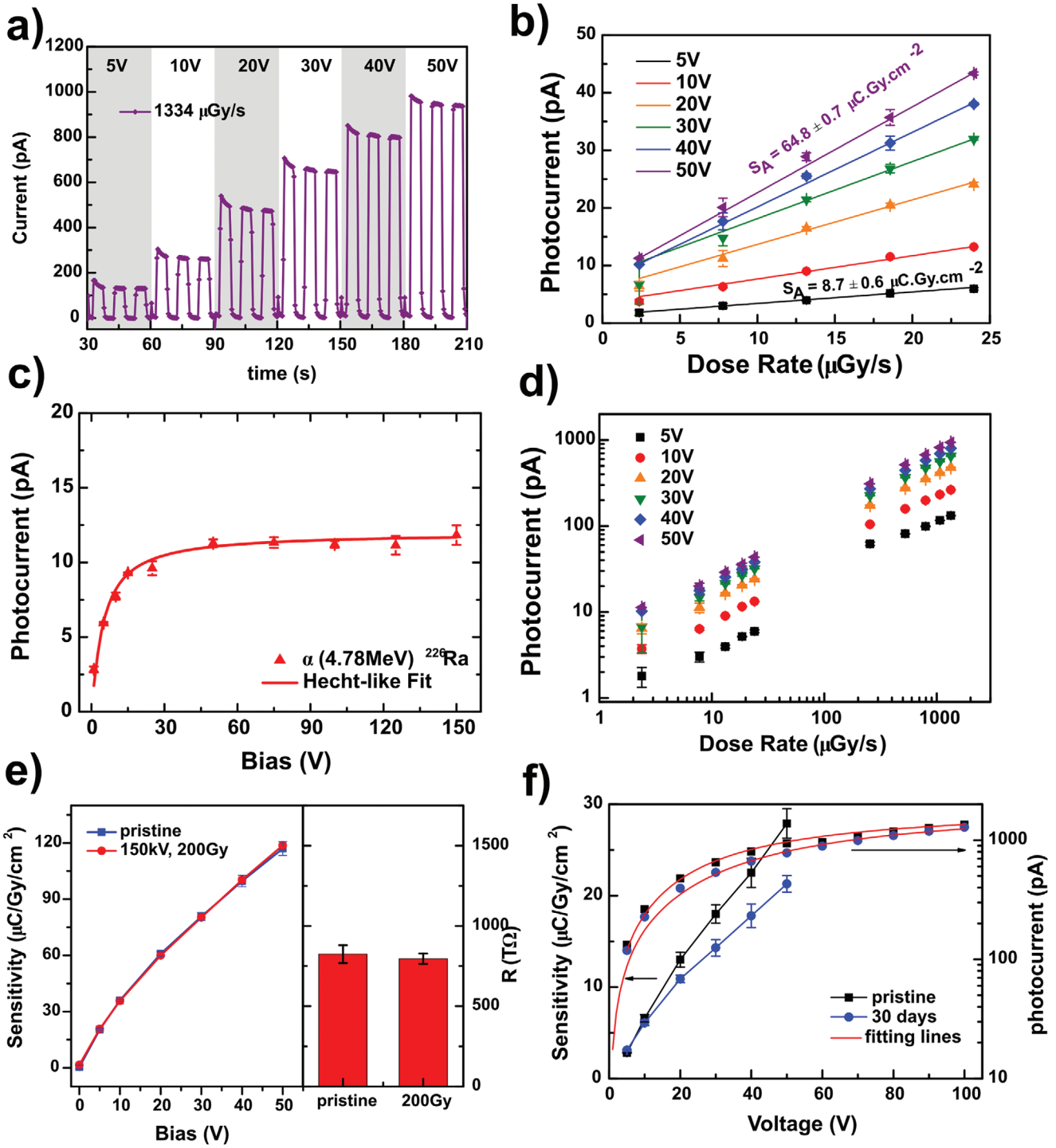

Figure 2. X-ray characterization, radiation hardness and aging. a) dynamic X-ray response at fixed dose rate of 1334 µGy s^{-1}, for bias 5, 10, 20, 30, 40, 50 V. X-ray source W-target at 40 kVp. b) Linearity of X-ray photocurrent versus dose rate and corresponding values of X-ray sensitivity. c) Photocurrent versus bias for alpha-emitting source of ^{226}Ra (red triangles) and corresponding Hecht-like fit (solid line). d) X-ray photocurrent versus dose rate in the range 2.5 – 1330 µGy s^{-1}. e) X-ray sensitivity versus applied bias (solid lines, left axis) and detectors resistance (vertical bars, right axis) for pristine crystals (blue) and after 200 Gy of X-ray at 150 kV (red). f) X-ray sensitivity (left axis) and photocurrent at 1330 µGy s^{-1} (right axis) at 40kVp versus applied bias for samples as-fabricated (t = 0, black dots) and after 30 days (blue dots).

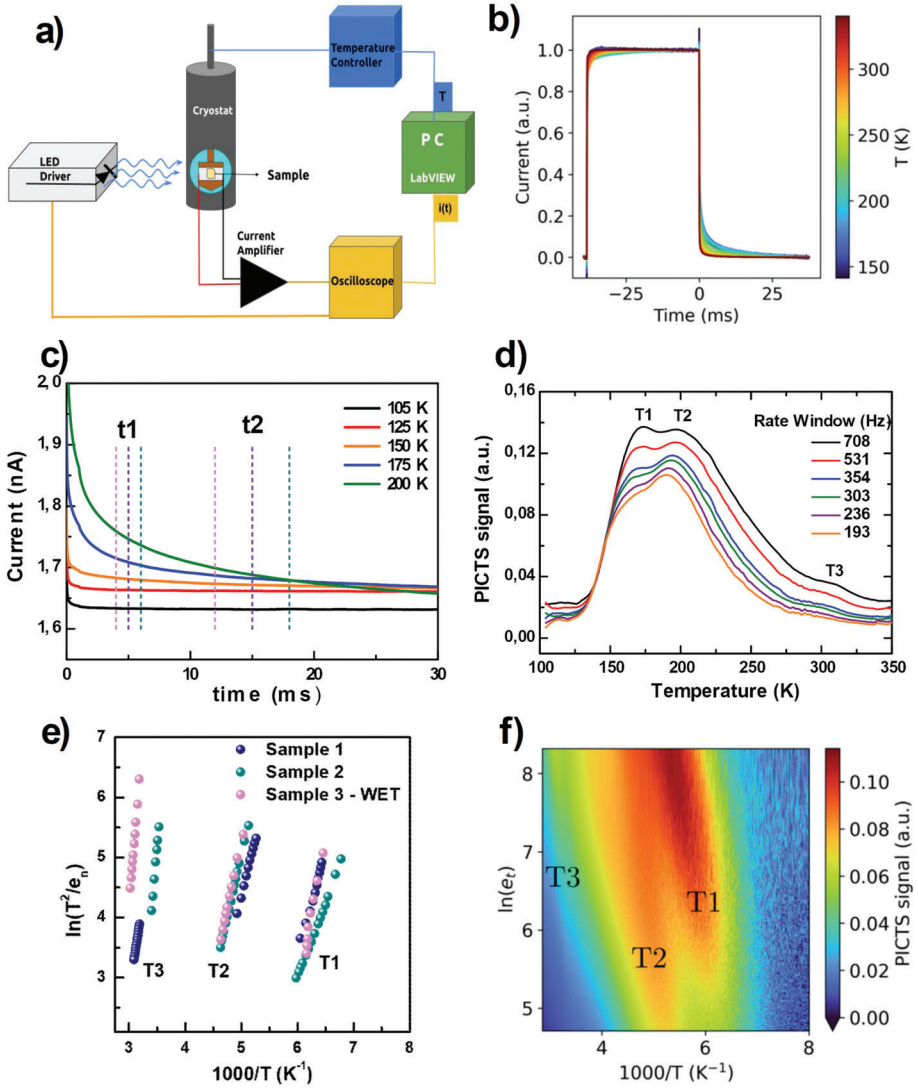

Figure 3. PICTS: identification of trap states. a) experimental setup for PICTS measurements. b) Normalized photocurrent pulses at different temperature at 13 Hz for PEA2PbBr4 crystal. c) Example of rate window applied to current transient of plot (b). d) PICTS spectra for selected rate window of 708, 531, 354, 303, 236 and 193 Hz in the range 100 – 350 K. e) Arrhenius plot for peak T1, T2 and T3 identified in PICTS spectra of (d). f) 2D colormap of $\ln(e_n)$ versus 1000/T as an alternative representation of Arrhenius plot.

2.2. Photo-Induced Current Transient Spectroscopy on PEA_2PbBr_4 Single Crystals

We have performed PICTS measurements on PEA_2PbBr_4 single crystals to investigate deep energy levels and to follow their evolution over time and under ionizing radiation. PICTS is a spectroscopic technique developed to study electrically active defects in highly resistive photoconductive materials, where the most common DLTS is not applicable. In a PICTS experiment, a pulsed optical excitation is used to generate charge carriers inside the material, allowing them to flow and fill intragap trap states. When the optical excitation is switched off, the relaxation transient of the electric current is measured through two ohmic contacts. Optical excitation and transient acquisition are repeated during a temperature scan (typically from 60 K to 450 K), allowing to extract the (thermal) activation energy of each identified deep trap. As the trap thermal emission rate (e_n) has a dependence with temperature (T) as follow:

$$e_n\ (T) = \gamma T^2 \sigma\, e^{-\frac{E_a}{k_B T}} \tag{2}$$

where, σ is the electron/hole capture cross-section, E_a is the level activation energy, and γ is a proportionality constant related to charge carriers' effective mass and to conduction/valence band availability. From the full dataset of current transients as function of temperature it is possible to experimentally identify specific levels, access their thermal emission rate e_n (or e_p for holes), and therefore measure the capture cross-section, and activation energy. **Figure 3a** shows a sketch of the PICTS experimental setup.

The ohmic behavior of samples under test have been verified (Figure SI 6a, Supporting Information), as it is an important requirement of PICTS. Perovskite samples are placed inside a cryostat with controlled temperature from liquid nitrogen temperature up to 450 K. A 365 nm LED illuminates the sample through an optical window, with a driving excitation frequency of 13 Hz and optical power of 14 mW cm^{-2}. The sample is biased at 10 V through a low noise current transimpedance amplifier connected to an oscilloscope to display and collect the output signal. Figure 3b shows the PEA_2PbBr_4 output current pulses taken at different temperatures, from 100 K to 340 K. The PICTS signal S is obtained from the relaxation transient in Figure 3b applying the rate window concept: we choose two successive instants during the relaxation transient, which start at t_0, such as $t_1 > t_0$ and $t_2 > t_1$, and express the PICTS signal as the difference in the value of the currents in these two instants, resulting in:

$$S\left(T, t_1, t_2\right) = i\left(T, t_1\right) - i\left(T, t_2\right) \quad (3)$$

as shown in Figure 3c. A typical PICTS spectrum resulting for PEA_2PbBr_4 is reported in Figure 3d in the temperature range from 100 K – 350 K for selected rate windows equal to $(t_2 - t_1)^{-1}$. Each pair of (t_1, t_2) has a biunivocal relation with emission rate e_n through a non-linear transcendental equation (see Technical Note S1, Supporting Information). If an electrically active trap state is present, thus giving a contribution to the photocurrent relaxation transient, a peak in the PICTS spectrum appears, corresponding to a specific emission rate. The emission rate of a trap state has a dependence with temperature T described by Equation, thus different rate windows are followed by a shift of the T_{max} of each peak. In the PICTS spectra of Figure 3d three peaks can be identified: we labeled them T1, T2 and T3. Despite a few DLTS spectra have been recently reported of 3D or mixed 2D/3D perovskite solar cells,[36,37] no other references for DLTS/PICTS on high-resistivity 2D perovskite spectra are known.

T1 and T2 are the two dominant peaks, visible in the temperature range between 150 – 180 K and 175 – 200 K, respectively. T3 is the least pronounced peak, but it clearly emerges at high-rate windows (i.e., high emission rates). Noteworthy, the PICTS spectrum results stable over multiple runs, meaning that continuous applied bias and pulsed light in vacuum for several hours and for multiple temperature ramps do not affect the material properties and response. The same technique applied to 3D perovskite crystals (like $MAPbBr_3$), where mixed electronic–ionic conduction governs the charge transport, yields photocurrent transients with much slower response and continuous variation in time under illumination, due to ionic charges redistribution.[21] The T_{max} and the corresponding e_n are plotted in the Arrhenius plot of Figure 3e where each series of points is associated to a specific trap state. From linear fits in the Arrhenius plot and following Equation it is possible to measure the activation energy E_a, reported in **Table 1**. Thermal transient techniques are powerful tools for the analysis of electrically active defects, with a high sensitivity even to small concentrations of trap states,[15,38] however, attention must be paid in the interpretation of peaks in the PICTS spectrum or in the Arrhenius plots to avoid misinterpretations due to artifacts associated to wrong choice of rate window.[39] To better display the full dataset in one plot, and to verify the reliability of our data, an alternative representation of an Arrhenius plot is presented in Figure 3f. Here a 2D colormap $ln(e_n)$ versus $1000/T$ represents all the possible combination of (e_n, T) for the acquired dataset.[40] In this representation, a trap state is characterized by a maximum in the 2D map whose values are stretched from high e_n at high temperature (top left in the plot) to lower e_n at lower temperature (bottom right in the plot). Every other maximum (symmetric peaks, horizontal/vertical lines, reverse shift) is an artefact to be excluded. The PICTS map confirms the correct interpretation of T1, T2 and T3. To summarize, in Table 1 are reported the activation energies of T1, T2 and T3 for two "*dry*" samples (fabricated as described above) and for one "*wet*" sample, which will be discussed later. All the three peaks are clearly identified in both *sample 1* and *sample 2*. While T1 and T2 are overlapped in the Arrhenius of Figure 3e, T3 varies from sample to sample and it is the most sensitive traps, as we will see later. Noteworthy, the level T2 could be compatible with an interstitial defect of bromide (Br_i) whose theoretical energy is expected at 0.34 eV from valence band (PEA_2PbBr_4 has dominant hole transport),[41] while T1 and T3 cannot be assigned at this stage.

Table 1. Activation energies of traps states from Arrhenius plot.

E_a [eV]	T1	T2	T3
Sample 1- dry	0.28 ± 0.01	0.32 ± 0.01	0.52 ± 0.08
Sample 2 – dry	0.22 ± 0.01	0.35 ± 0.02	0.92 ± 0.02
Sample 3 – wet	0.38 ± 0.04	0.33 ± 0.01	0.97 ± 0.02

After having assessed that PICTS can successfully identify and characterize deep levels in 2D perovskites, we used this technique to investigate radiation tolerance and environmental effects on traps states, that can be correlated with the observed macroscopic stability in the device performance in Figure 2e,f. The ionizing radiation effects on defect levels in *sample 1* have been evaluated using the following protocol. i) A first PICTS measurement has been performed on pristine crystal. ii) A second measurement was repeated after ≈2 weeks to assess the stability of the sample. iii) Immediately after the second run, the sample was irradiated with a dose of 200 Gy of X-ray at 150 kVp, and then tested again with a third PICTS run. A direct comparison of three PICTS spectra taken for each one of the above steps (identical rate window) and the corresponding Arrhenius plots are shown in **Figure 4a,b**. The complete spectra evolution for various rate windows and corresponding PICTS maps are reported in Figure SI 3 (Supporting Information). Figure 4a,b shows a substantial stability of peaks T1 and T2 even after strong X-ray irradiation, while T3 becomes more prominent after X-ray irradiation. Levels T1 and T2 have completely overlapping Arrhenius plots and their activation energy is very stable both over two weeks of ambient storage and after X-ray irradiation (**Table 2**). On the other hand, the E_a of level T3 shifts of 0.1 eV after a two-week storage, and dramatically changes under ionizing radiation, presenting a very pronounced peak with E_a = 2.2 eV (Figure 4a,b). Such a strong modification could suggest that an additional state has been activated. Noteworthy, the absolute photocurrent saturation value recorded under 365 nm LED irradiation varies between pristine and irradiated samples, and the PICTS/saturation current ratio is proportional to relative trap concentrations.[42,43] Figure 4b emphasizes that, while the energy level of the traps remains

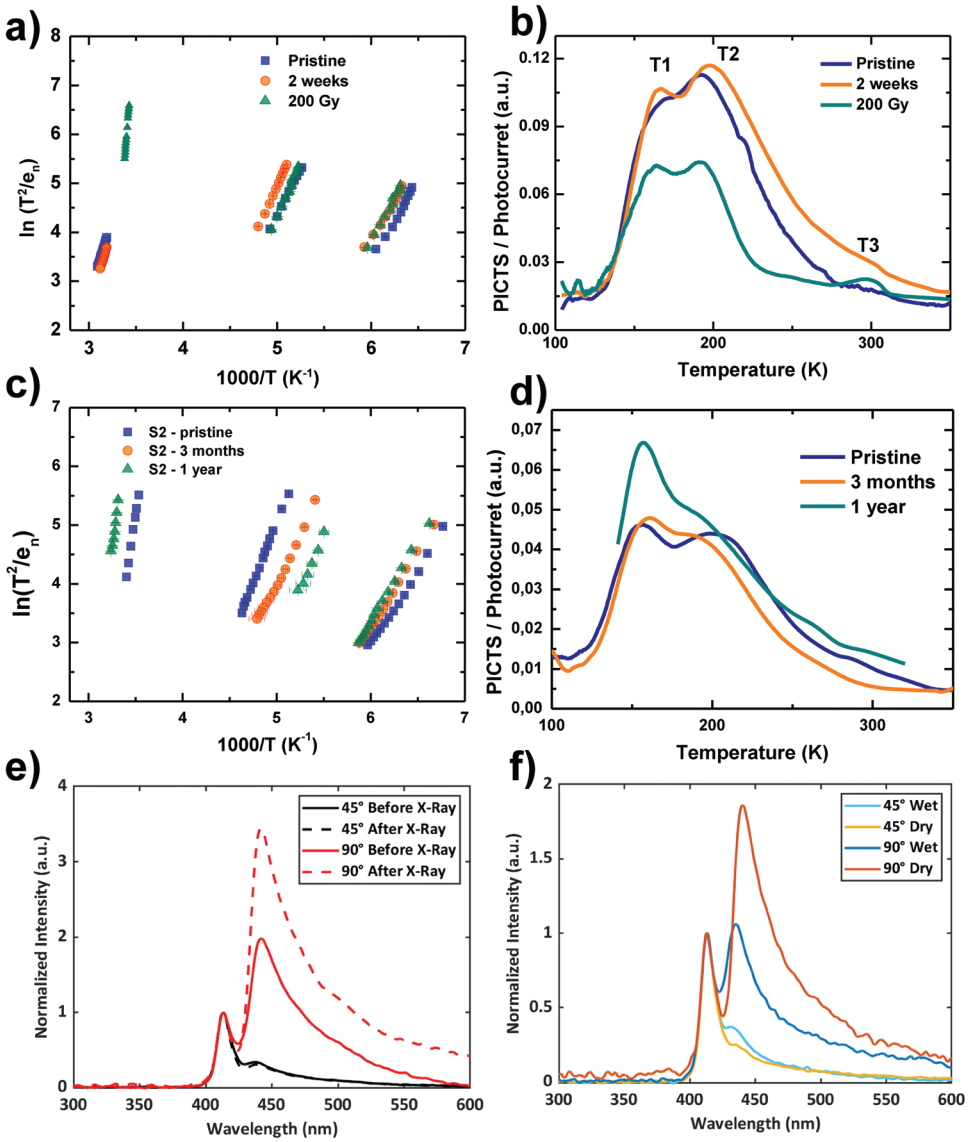

Figure 4. Trap states stability: radiation tolerance and aging. a,b) Arrhenius plot (a) and PICTS signal/photocurrent at 265 Hz (b) of sample 1 for pristine (blue), after 2 weeks (orange) and after 200 Gy of X-ray (green). c,d) Arrhenius plot (c) and PICTS signal/photocurrent at 265 Hz (d) of sample 2 for pristine (blue), after 3 months (orange) and after 1 year (green). e,f) Photoluminescence spectra of PEA_2PbBr_4 crystals collected at angle 45° (black) and 90° (red) respect to the incident pumping laser. e) Before (solid line) and after 200 Gy of X-ray (dashed line); f) for sample 2 – dry (yellow and red lines) and sample 3 – wet (light blue and blue lines) crystals.

Table 2. Activation energies of levels T1, T2 and T3 calculated from Figure 4.

E_a [eV]	T1	T2	T3
Pristine	0.28 ± 0.01	0.32 ± 0.01	0.52 ± 0.08
Two weeks	0.31 ± 0.01	0.37 ± 0.01	0.62 ± 0.08
X-rays	0.29 ± 0.01	0.37 ± 0.01	2.2 ± 0.3
Pristine	0.22 ± 0.01	0.35 ± 0.02	0.92 ± 0.02
3 months	0.23 ± 0.01	0.30 ± 0.01	n/a
1 year	0.23 ± 0.01	0.32 ± 0.02	1.02 ± 0.09
Wet	0.38 ± 0.04	0.33 ± 0.01	0.97 ± 0.02

unchanged, their concentration is affected by X-rays with a generalized reduction of relative trap concentrations. Interestingly, the photocurrent transient is faster in the irradiated samples (Figure SI 4, Supporting Information), and it is a phenomenon generally associated with the presence of a lower density of trap states. The reduction in trap concentration (i.e., the decrease of the normalized peak intensity) is more pronounced for T1 and T2, while T3 emerges from the irradiated PICTS spectrum in Figure 4b.

In *sample 2*, we followed the evolution of the PICTS spectrum of the same samples during a period of one year to evaluate the long-term aging effects. The samples were stored in standard ambient condition during the whole year, and their dark

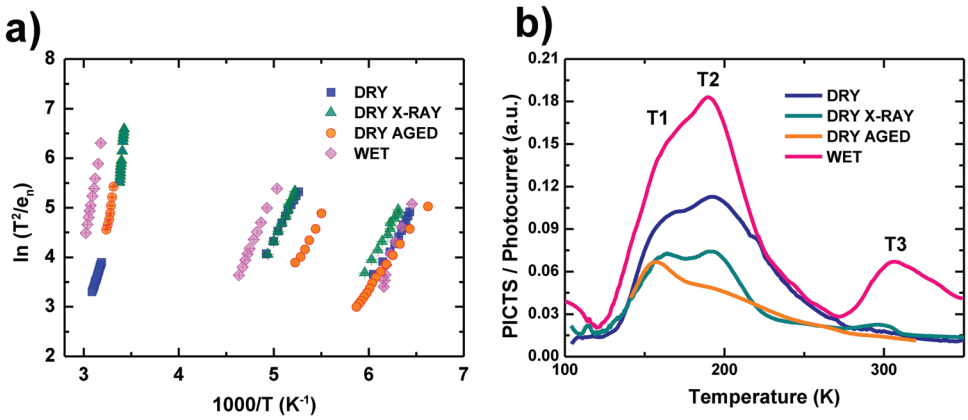

Figure 5. Wet crystals. Arrhenius plot (a) and normalized PICTS signal/photocurrent at 265 Hz (b) of pristine dry (blue), dry after 200 Gy (green) and wet sample (pink).

current remained stable (Figure SI 6b, Supporting Information). Figure 4c,d report the Arrhenius plots and the relative traps concentration (PICTS/photocurrent spectrum) for pristine crystal, after 3 months and after 1 year. The level T1 results to be the most stable, showing data points in the Arrhenius plot of Figure 4c perfectly superimposed and no difference in trap concentrations within 3 months. The level T2 slightly reduces its relative concentration after 3 months but its activation energy is stable, as the slight variation of E_a is within experimental errors. After 1 year, the relative concentration of T1 increases, while the activation energies of both T1 and T2 are stable. Level T3 has a peculiar evolution. It is detectable in the pristine sample, after 3 months its concentration decreases below the detection limit of the technique and then increases again, as after 1 year a broad peak with relative trap concentration above the pristine condition is recorded.

PL measurements provide additional information on the trap states, helpful for the identification of T1, T2 and T3. Figure 4e reports the photoluminescence properties of *sample 1* before and after X-ray irradiation. No significant differences are observed in the spectra at 45° configuration, dominated by surface related excitation. On the contrary, at 90° configuration the light penetrates deeper in the bulk and the intensity of the peak at 435 nm clearly increases after X-ray irradiation. The enhancement of PL emission in perovskites is generally associated to a reduction of self-absorption, correlated to the presence of deep trap states that absorb the light.[23,44] The rising of bulk-related PL emission is thus in line with the generalized reduction of deep traps concentration observed in the PICTS spectrum after X-ray irradiation, reported in Figure 4b. Additionally, the two-year-old PL spectrum of *sample 2* (*dry* plots in Figure 4e) displays the same peaks and features of the as-grown crystal reported in Figure 1c, confirming the considerable time stability, as expected when comparing these results with the small variations observed in the PICTS spectrum of one-year-old sample.

Overall, following the above discussion of the reported results, we can infer that level T1 and T2 are traps mainly related to the material intrinsic properties, which are stable over at least 1 year. Level T3 has variable behavior, it is present in lower concentration with respect to T1 and T2 and, importantly, plays a minor role in the macroscopic detector performance.

2.3. *Wet*, Highly Defective PEA_2PbBr_4 Crystals

It is well known that environmental humidity has a strong impact in perovskite opto-electronics characteristics,[45] and 2D perovskites, even if less reactive than 3D ones, do not make an exception. To identify the role of water molecules, we prepared a *"wet"* crystal (*sample 3*), i.e., an excess of 150 nL of water was added to the starting solution, thus these crystals grew in an environment with very high-water content. The surface of one of such *wet* crystals is extremely rough (Figure SI 1c, Supporting Information) and the 90° polarized light displays several bright zones of crystalline cracks (Figure SI 1d, Supporting Information). Numerous large features are visible with WLI microscope on the surface, with several plane discontinuities, at least five different crystalline planes, with total step height above 50 µm, (Figure SI 2, Supporting Information). The highly defective structure of *wet* crystals is macroscopically confirmed by the comparison of PL emission intensity of *dry* crystals, reported in Figure 4f under the same excitation conditions. No substantial differences are observed when the surface emission dominates (PL at 45°). However, at 90° (i.e., when bulk emission dominates), the highly defective *wet* sample exhibits a peak intensity that is only half in comparison with the *dry* sample, suggesting the presence in the *wet* sample of bulk defects causing strong self-absorption of emitted light. A comparison of the optoelectronic characterization of a *dry* and a *wet* sample (Table SI 1, Supporting Information), provides quite interesting insights. First, the *wet* sample resistance in dark is two orders of magnitude higher than the *dry* one, as the high concentration of trap states reduces the effective mobility of the charge carriers. On the opposite, UV photocurrent signal, responsivity and specific detectivity are much higher in the *wet*, more defective crystal than in the *dry* one, suggesting that the mechanism of photocurrent generation is strongly trap-assisted in PEA_2PbBr_4 crystals. Regrettably, contrary to what has been assessed for *dry* crystals, *wet* more defective crystals are strongly affected by ageing, as their optoelectronic properties are completely degraded after two years.

The PICTS spectrum of *sample* 3 – *wet* shows three peaks corresponding to T1, T2 and T3 levels (**Figure** 5a,b). It shows a higher concentration for all the traps, as highlighted by the high values of PICTS/Photocurrent in Figure 4f, with respect to the *dry*

crystals we have discussed so far (*sample 1* and *sample 2*). Even in such a highly defective crystal, levels T1 and T2 are clearly identified also in the Arrhenius plot, with small variation of E_a values respect to *sample 1* and *sample 2*.

2.4. Trap States: Origin and Nature

The results obtained from *dry* and *wet* PEA_2PbBr_4 crystals exposed both to 200 Gy of X-ray radiation at 150kVp and to aging up to 1 year, allow us to propose an identification of the observed deep trap states. We do not know the origin of T1, but, based on energetic consideration of simulated point defects,[41] we could tentatively assign T2 to Br interstitials. In addition, in our recent paper we proposed that comparable X-ray exposure of $MAPbBr_3$ single crystals creates Br vacancies.[27] If an analogous effect also occurs in PEA_2PbBr_4 crystals, we could speculate that the X-ray induced Br vacancies balance the Br interstitial defective states already present in the as-grown crystal, resulting in a net reduction of the total concentration of trap states. From the comparison of *dry* and *wet* PEA_2PbBr_4 crystals, we tentatively assign the trap state T3 to the interaction of water with the perovskite lattice. It is noteworthy that the peak corresponding to T3 is strongly pronounced and dominant in the high temperature region of the PICTS spectrum of *wet* samples and that its activation energy agrees with the one of the X-rayed and 1-year aged samples (Figure 4e and Table 2). This last observation suggests that environmental stress effects on 2D PEA_2PbBr_4 perovskite are triggered and associated to the interaction with water molecules, as both *wet* and aged samples have a significant concentration of level T3.

Additional information on the disorder regime of each trap state could be determined by the broadening of the PICTS peaks,[46] as detailed in Technical Note S2 (Supporting Information). The here reported results indicate that trap states T1 and T3 are clearly in the weak disorder regime, (as $\sigma/E_0 < 0.1$) and that no distribution of multiple activation energies should be considered. More caution should be used for the interpretation of T2, as its large peak broadening ($\sigma/E_0 = 0.21$, particularly pronounced toward higher temperatures) could hide a more complex wide- or multi-band structure.

3. Conclusion

We grew from solution 2D layered PEA_2PbBr_4 perovskite single crystals to study electrically active defect states in such material systems. First, we showed that such crystals are promising and reliable candidates for UV–vis and real-time direct X-ray detectors (for energies from 40 to 150 kVp), thanks to their very low dark current, high quality optoelectronic properties and stability to aging and radiation harsh environment. Then, we used PICTS technique to investigate their electrically active defective states. Three levels have been identified within the bandgap: i) T1 with $E_a = 0.26$ eV, of still unknown origin; ii) T2 with $E_a = 0.33$ eV, that we tentatively assigned to Br interstitials; iii) T3 with a variable activation energy and a non-constant presence in PICTS spectra. Considering the large E_a variation (0.52 – 2.2 eV), we refrain from assigning it a specific value, but we could relate its presence to the interaction of perovskite with H_2O molecules. Overall, levels T1 and T2 showed a great stability and robustness, as the PEA_2PbBr_4 perovskite crystals, exposed both to 200 Gy of X-ray radiation at 150kVp and to aging up to 1 year, maintain their optoelectronic and radiation detecting properties.

Supporting Information

Supporting Information is available from the Wiley Online Library or from the author.

Acknowledgements

L.M. has been financed under a research contract co-financed by the European Union under – PON Ricerca e Innovazione 2014–2020, art. 24, comma 3, lett. a), della Legge 30 dicembre 2010, n. 240 e s.m.i. e del D.M. 10 agosto 2021 n. 1062″. This work also received funding from the PROGETTO DI RICERCA DI RILEVANTE INTERESSE NAZIONALE (PRIN 2022 PNRR) n. P2022ACY8P A Multicomponent Solar Energy Conversion System with Extended Spectral Collection and Improved Efficiency (MUSES). The authors also acknowledge Dr. Ferdinand Lédée for sharing the recipe of crystal's growth used by the authors in this work.

Open access publishing facilitated by Universita degli Studi di Bologna, as part of the Wiley - CRUI-CARE agreement.

Conflict of Interest

The authors declare no conflict of interest.

Data Availability Statement

The data that support the findings of this study are available from the corresponding author upon reasonable request.

Keywords

deep levels, defects, low-dimensional perovskites, perovskites, PICTS, radiation hardness

Received: March 27, 2024
Revised: August 21, 2024
Published online:

[1] H. Tsai, W. Nie, J.-C. Blancon, C. C. Stoumpos, R. Asadpour, B. Harutyunyan, A. J. Neukirch, R. Verduzco, J. J. Crochet, S. Tretiak, L. Pedesseau, J. Even, M. A. Alam, G. Gupta, J. Lou, P. M. Ajayan, M. J. Bedzyk, M. G. Kanatzidis, A. D. Mohite, *Nature* **2016**, *536*, 312.

[2] T. Campos, P. Dally, S. Gbegnon, A. Blaizot, G. Trippé-Allard, M. Provost, M. Bouttemy, A. Duchatelet, D. Garrot, J. Rousset, E. Deleporte, *J. Phys. Chem. C* **2022**, *126*, 13527.

[3] S. Sidhik, Y. Wang, M. De Siena, R. Asadpour, A. J. Torma, T. Terlier, K. Ho, W. Li, A. B. Puthirath, X. Shuai, A. Agrawal, B. Traore, M. Jones, R. Giridharagopal, P. M. Ajayan, J. Strzalka, D. S. Ginger, C. Katan, M. A. Alam, J. Even, M. G. Kanatzidis, A. D. Mohite, *Science* **2022**, *377*, 1425.

[4] A. H. Proppe, A. Johnston, S. Teale, A. Mahata, R. Quintero-Bermudez, E. H. Jung, L. Grater, T. Cui, T. Filleter, C.-Y. Kim, S. O. Kelley, F. De Angelis, E. H. Sargent, *Nat. Commun.* **2021**, *12*, 3472.

[5] L. Basiricò, I. Fratelli, M. Verdi, A. Ciavatti, L. Barba, O. Cesarini, G. Bais, M. Polentarutti, M. Chiari, B. Fraboni, *Adv. Sci.* **2023**, *10*, 2204815.
[6] Y. J. Hofstetter, I. García-Benito, F. Paulus, S. Orlandi, G. Grancini, Y. Vaynzof, *Frontiers in Chem.* **2020**, *8*.
[7] T. L. Leung, I. Ahmad, A. A. Syed, A. M. C. Ng, J. Popović, A. B. Djurišić, *Commun. Mater.* **2022**, *3*, 63.
[8] Y. Zhang, Y. Liu, Z. Xu, H. Ye, Q. Li, M. Hu, Z. Yang, S. (Frank) Liu, *J. Mater. Chem. C* **2019**, *7*, 1584.
[9] F. Lédée, A. Ciavatti, M. Verdi, L. Basiricò, B. Fraboni, *Adv. Opt. Mater.* **2022**, *10*, 2101145.
[10] H. Tsai, S. Shrestha, L. Pan, H.-H. Huang, J. Strzalka, D. Williams, L. Wang, L. R. Cao, W. Nie, *Adv. Mater.* **2022**, *34*, 2106498.
[11] H. Tsai, F. Liu, S. Shrestha, K. Fernando, S. Tretiak, B. Scott, D. T. Vo, J. Strzalka, W. Nie, *Sci. Adv.* **2020**, *6*, eaay0815.
[12] X. He, M. Xia, H. Wu, X. Du, Z. Song, S. Zhao, X. Chen, G. Niu, J. Tang, *Adv. Funct. Mater.* **2022**, *32*, 2109458.
[13] H. Li, J. Song, W. Pan, D. Xu, W. Zhu, H. Wei, B. Yang, *Adv. Mater.* **2020**, *32*, 2003790.
[14] Y. Chen, Y. Sun, J. Peng, J. Tang, K. Zheng, Z. Liang, *Adv. Mater.* **2018**, *30*, 1703487.
[15] D. V. Lang, *J. Appl. Phys.* **1974**, *45*, 3023.
[16] P. Blood, J. W. Orton, *The Electrical Characterization of Semiconductors: Majority Carriers and Electron States*, Academic Press, Cambridge, Massachusetts **1992**.
[17] V. Pecunia, J. Zhao, C. Kim, B. R. Tuttle, J. Mei, F. Li, Y. Peng, T. N. Huq, R. L. Z. Hoye, N. D. Kelly, S. E. Dutton, K. Xia, J. L. MacManus-Driscoll, H. Sirringhaus, *Adv. Energy Mater.* **2021**, *11*, 2003968.
[18] J. A. Peters, Z. Liu, M. C. De Siena, M. G. Kanatzidis, B. W. Wessels, *J. Appl. Phys.* **2022**, *132*, 035101.
[19] M. H. Futscher, C. Deibel, *ACS Energy Lett.* **2022**, *7*, 140.
[20] M. Verdi, A. Ciavatti, J. Segura-Ruiz, L. Basiricò, R. Sorrentino, I. P. Goncalves, A. Petrozza, F. Boscherini, B. Fraboni, *Adv. Electron. Mater.* **2023**, *9*, 2201346.
[21] G. Armaroli, L. Maserati, A. Ciavatti, P. Vecchi, A. Piccioni, M. Foschi, V. Van der Meer, C. Cortese, M. Feldman, V. Foderà, T. Lemercier, J. Zaccaro, J. M. Guillén, E. Gros-Daillon, B. Fraboni, D. Cavalcoli, *ACS Energy Lett.* **2023**, *10*, 4371.
[22] J. C. Balland, J. P. Zielinger, C. Noguet, M. Tapiero, *J. Phys. D: Appl. Phys.* **1986**, *19*, 57.
[23] Q. Du, C. Zhu, Z. Yin, G. Na, C. Cheng, Y. Han, N. Liu, X. Niu, H. Zhou, H. Chen, L. Zhang, S. Jin, Q. Chen, *ACS Nano* **2020**, *14*, 5806.
[24] T. Jin, Z. Liu, J. Luo, J.-H. Yuan, H. Wang, Z. Xie, W. Pan, H. Wu, K.-H. Xue, L. Liu, Z. Hu, Z. Zheng, J. Tang, G. Niu, *Nat. Commun.* **2023**, *14*, 2808.
[25] W. Peng, J. Yin, K.-T. Ho, O. Ouellette, M. De Bastiani, B. Murali, O. El Tall, C. Shen, X. Miao, J. Pan, E. Alarousu, J.-H. He, B. S. Ooi, O. F. Mohammed, E. Sargent, O. M. Bakr, *Nano Lett.* **2017**, *17*, 4759.
[26] R. J. Elliott, *Phys. Rev.* **1957**, *108*, 1384.
[27] G. Armaroli, L. Ferlauto, F. Lédée, M. Lini, A. Ciavatti, A. Kovtun, F. Borgatti, G. Calabrese, S. Milita, B. Fraboni, D. Cavalcoli, *ACS Appl. Mater. Interfaces* **2021**, *13*, 58301.
[28] Y. Lin, Y. Bai, Y. Fang, Q. Wang, Y. Deng, J. Huang, *ACS Energy Lett.* **2017**, *2*, 1571.
[29] X. Xiao, J. Dai, Y. Fang, J. Zhao, X. Zheng, S. Tang, P. N. Rudd, X. C. Zeng, J. Huang, *ACS Energy Lett.* **2018**, *3*, 684.
[30] Y. Fang, A. Armin, P. Meredith, J. Huang, *Nat. Photon* **2019**, *13*, 1.
[31] K. Hecht, *Z. Physik* **1932**, *77*, 235.
[32] A. Ciavatti, P. J. Sellin, L. Basiricò, A. Fraleoni-Morgera, B. Fraboni, *Appl. Phys. Lett.* **2016**, *108*, 153301.
[33] K.-O. Kim, T.-J. Kwon, J. K. Kim, J.-H. Ha, *J. the Korean Phys. Soc.* **2011**, *59*, 20.
[34] O. Semeniuk, O. Grynko, G. Decrescenzo, G. Juska, K. Wang, A. Reznik, *Sci. Rep.* **2017**, *7*, 8659.
[35] L. Basiricò, S. P. Senanayak, A. Ciavatti, M. Abdi-Jalebi, B. Fraboni, H. Sirringhaus, *Adv. Funct. Mater.* **2019**, *29*, 1902346.
[36] S. Heo, G. Seo, K. T. Cho, Y. Lee, S. Paek, S. Kim, M. Seol, S. H. Kim, D.-J. Yun, K. Kim, J. Park, J. Lee, L. Lechner, T. Rodgers, J. W. Chung, J.-S. Kim, D. Lee, S.-H. Choi, M. K. Nazeeruddin, *Adv. Energy Mater.* **2019**, *9*, 1902470.
[37] C. Bao, F. Gao, *Rep. Prog. Phys.* **2022**, *85*, 096501.
[38] J. A. Borsuk, R. M. Swanson, *IEEE Trans. Electron Devices* **1980**, *27*, 2217.
[39] J. Siekmann, S. Ravishankar, T. Kirchartz, *ACS Energy Lett.* **2021**, *6*, 3244.
[40] J. V. Li, *Rev. Sci. Instrum.* **2021**, *92*, 023902.
[41] J. Yin, R. Naphade, L. Gutiérrez Arzaluz, J.-L. Brédas, O. M. Bakr, O. F. Mohammed, *ACS Energy Lett.* **2020**, *5*, 2149.
[42] B. Fraboni, R. DiPietro, A. Cavallini, P. Cosseddu, A. Bonfiglio, J. O. Vogel, *Appl. Phys. A* **2008**, *95*, 37.
[43] A. Cavallini, B. Fraboni, W. Dusi, M. Zanarini, P. Siffert, *Appl. Phys. Lett.* **2000**, *77*, 3212.
[44] X. Gong, O. Voznyy, A. Jain, W. Liu, R. Sabatini, Z. Piontkowski, G. Walters, G. Bappi, S. Nokhrin, O. Bushuyev, M. Yuan, R. Comin, D. McCamant, S. O. Kelley, E. H. Sargent, *Nat. Mater.* **2018**, *17*, 550.
[45] Z. Zhu, V. G. Hadjiev, Y. Rong, R. Guo, B. Cao, Z. Tang, F. Qin, Y. Li, Y. Wang, F. Hao, S. Venkatesan, W. Li, S. Baldelli, A. M. Guloy, H. Fang, Y. Hu, Y. Yao, Z. Wang, J. Bao, *Chem. Mater.* **2016**, *28*, 7385.
[46] A. Das, V. A. Singh, D. V. Lang, *Semicond. Sci. Technol.* **1988**, *3*, 1177.